Soils and Foundations 2013;53(6):951–965

The Japanese Geotechnical Society

Soils and Foundations

www.sciencedirect.com
journal homepage: www.elsevier.com/locate/sandf

Strength and deformation characteristics and small strain properties of undisturbed gravelly soils

Tadao Enomoto[a,*,1], Obaid Hassan Qureshi[b,1], Takeshi Sato[c], Junichi Koseki[d]

[a]*Public Works Research Institute, Japan*
[b]*READ Foundation, Pakistan*
[c]*Integrated Geotechnology Institute Limited, Japan*
[d]*Institute of Industrial Science, University of Tokyo, Japan*

Received 18 February 2013; received in revised form 4 June 2013; accepted 24 July 2013
Available online 23 November 2013

Abstract

A series of medium-scale and large-scale triaxial and unconfined compression tests was conducted in order to evaluate the strength and deformation characteristics and small strain properties of undisturbed well-graded gravelly soils retrieved from three tunnel excavation sites in Toyama prefecture, Japan. Undisturbed gravelly soils were taken by means of a new sampling method using thick water-soluble polymer solutions. The strength and deformation characteristics were evaluated mainly by performing sustained loading and large amplitude unloading and reloading cycles during otherwise monotonic loading at a constant strain rate in drained triaxial compression tests. During isotropic consolidation and shearing, at several stress states, eleven very small vertical cycles were applied to evaluate the quasi-elastic deformation property at small strain levels around 0.001% by static measurement. Dynamic measurements using a pair of accelerometers attached to the side surface of the specimen and wave sources attached to the top cap were also conducted at the same stress levels as static measurements in a single test. Several effects including grading characteristics and pressure level on the difference between the moduli measured statically and dynamically were discussed. The relationship between the small strain and strength properties of undisturbed gravelly soils was evaluated. The small strain properties of air-dried dense Toyoura sand in large-scale triaxial compression tests were also investigated in this study to compare the results of undisturbed gravelly soils.

Keywords: Strength and deformation characteristics; Small strain stiffness; Static and dynamic measurements; Undisturbed gravelly soil; Triaxial compression; IGC: D6; D7

1. Introduction

The strength and deformation characteristics of gravelly soils (denoted as GSs) have been studied for about half a century in order to investigate their use in the large-scale structures such as rockfill dams and embankments (e.g., Holtz and Gibbs, 1956; Jiang et al., 1997; Okuyama et al., 2003). These experimental studies were mainly conducted under reconstituted conditions; however, the number of studies on undisturbed gravelly soils (UGSs) is limited due to technical problems in sampling methods for in-situ samples with cobbles and boulders. If the conventional sampling methods for

*Corresponding author.
E-mail address: enomoto@pwri.go.jp (T. Enomoto).
[1]Formerly Graduate Student, Department of Civil Engineering, University of Tokyo, Japan.
Peer review under responsibility of The Japanese Geotechnical Society.

Production and hosting by Elsevier

0038-0806 © 2013 The Japanese Geotechnical Society. Production and hosting by Elsevier B.V. All rights reserved.
http://dx.doi.org/10.1016/j.sandf.2013.10.004

Nomenclature

a	parameter on inherent anisotropy
c	cohesion
d	specimen diameter
D	partical diameter
D_{50}	mean particle diameter
D_{max}	maximum particle diameter
D_{r0}	initial relative density
E_{max}	maximum secant Young's modulus
E_{sec}	secant Young's modulus
E_{tan}	tangential Young's modulus
E_{v0}	reference vertical Young's modulus at a reference stress state
E_{vs}	quasi-elastic vertical Young's modulus by static measurement
FC	fines content
G_{vh0}	reference shear modulus at a reference stress state
G_{vhd}	shear modulus by dynamic measurement
G_{vhs}	shear modulus converted from E_{vs}
$(G_{vhd}/G_{vhs})_{50}$	G_{vhd}/G_{vhs} at isotropic stress state of $\sigma'_v=\sigma'_h=50$ kPa
h	specimen height
L	distance between the sampling location and the borehole where in-situ PS logging test was conducted
m	parameter presenting stress-state dependency of E_{vs}
m'	parameter presenting stress-state dependency of shear modulus
m_d'	m' by dynamic measurement
m_s'	m' based on static measurement
p'	effective mean stress $=(\sigma'_v+2\sigma'_h)/3$
q	deviator stress
q_{max}	maximum deviator stress
R	effective principal stress ratio$=\sigma'_v/\sigma'_h$
U_c	coefficient of uniformity
$V_{s(dynamic)}$	shear wave velocity by dynamic measurement
$V_{s(static)}$	equivalent shear wave velocity converted from G_{vhs}
Δt_{peak}	peak-to-peak travel time
Δt_{rise}	rise-to-rise travel time
$\Delta\varepsilon_v$	vertical strain increment
σ'_3	effective minor principal stress
σ'_h	effective horizontal principal stress
σ'_v	effective vertical principal stress
$\dot{\sigma}'_v$	effective vertical principal stress rate
ε_h	horizontal strain
ε_v	vertical strain
ε_{vol}	volumetric strain
$\dot{\varepsilon}_v$	vertical strain rate
ϕ	internal friction angle
λ	wave length in dynamic measurement
υ_0	Poisson's ratio at isotropic stress state
ρ_d	initial dry density of specimen
ρ_t	wet density of specimen

relatively finer geomaterials are used for GSs, positions of large particles may be moved largely during the coring process. Some studies using UGSs retrieved by the in-situ freezing method developed to provide temporary particle bonding were conducted (e.g., Nishio and Tamaoki,1988; Goto et al., 1992; Yasuda et al., 1994; Tanaka et al., 2000). However, this sampling method is in general costly, in particular with large diameter samples, and also may not be applicable if fine particles are included. In view of the above, by taking advantage of a newly developed sampling method using thick water-soluble polymer solutions (Tani et al., 2007), UGSs were retrieved from three tunnel excavation sites in Toyama prefecture, Japan.

Soil characteristics at a small strain level are important in order to predict the overall deformation behaviour and have been studied by many researchers (e.g., Jardine and Potts, 1988; Tatsuoka and Shibuya, 1992; Kohata et al., 1997; Fioravante, 2000; AnhDan et al., 2002). The methods to evaluate small strain properties experimentally are divided into static and dynamic ones. The soil behaviour observed by applying many small unload/reload cycles of axial stress statically in the laboratory tests is essentially linear and nearly recoverable within a very small strain range lesser than 0.001% (Tatsuoka and Shibuya, 1992). For this static measurement, the experimental devices have to be very precise and accurate. On the other hand, the main method to evaluate small strain stiffness dynamically in the laboratory is the use of bender element (e.g., Brignoli et al., 1996; Fioravante, 2000; Leong et al., 2005). However, in this method, the disturbance induced by inserting the plates into soil specimens as well as the effects of bedding error have a negative influence on the accurate evaluation of small strain properties (Wicaksono et al., 2008). In addition, this method may not be applicable to GSs with large particles due to its limited capacity of excitation and insufficient contact between the plates and coarse soil particles. In view of the above, the precise equipment for measurements of axial loading and deformation (e.g., Tatsuoka and Shibuya, 1992; AnhDan et al., 2002) and a new technique originally developed by AnhDan et al. (2002) were used for static and dynamic measurements, respectively.

In order to evaluate the strength and deformation characteristics and small strain properties of UGSs mentioned above, a series of medium-scale and large-scale triaxial and unconfined compression (TC and UC, respectively) tests with static and dynamic measurements was conducted. Small strain properties of air-dried dense Toyoura sand in large-scale TC tests were also investigated to compare with those of UGSs.

2. Tested materials and their sampling

The tested UGSs were retrieved from construction sites of Makurano, First Uozu and Second Uozu Tunnels (MT, FUT and SUT, respectively) for Hokuriku bullet train, in Toyama prefecture, Japan.

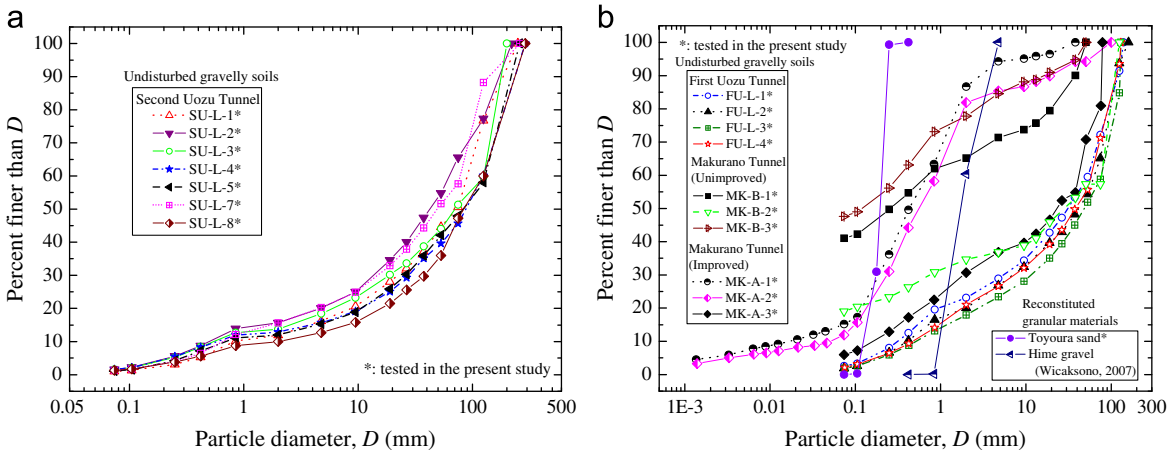

Fig. 1. Some of the grading curves of geomaterials referred to in this paper: (a) UGSs retrieved from SUT and (b) UGSs retrieved from FUT and MT and reconstituted materials.

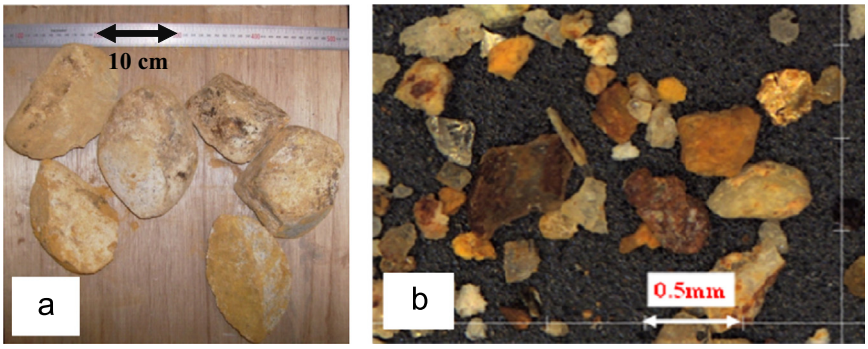

Fig. 2. Typical components of different particle sizes of UGS retrieved from FUT: (a) large particles and (b) small particles.

Fig. 1 shows some of the grading curves of geomaterials tested and referred to in this paper. Fig. 2 shows the typical particle pictures of UGS retrieved from FUT. The values of mean diameter (D_{50}), maximum diameter (D_{max}), uniformity coefficient (U_c), fines content (FC), initial dry density (ρ_d) and specimen diameter (d) are listed in Table 1. The ρ_d values of UGSs were estimated by the average water contents of specimens after TC or UC tests.

At FUT and SUT, as mentioned in the introduction, a special coring method was used for the retrieval of UGSs. This sampling technique is a non-freezing sampling method using thick water-soluble polymer solutions and a single steel tube sampler which has diamond bits at its bottom for cutting, where the bits can cut large particles without moving their positions largely. The samples can be protected by covering them with the polymer solutions during the coring work. In addition, since the shear stress acting on the sample surface during the coring work is very small due to the shear-thinning effects of the polymer solutions, the soil fabric in the samples can also be maintained (Tani et al., 2007). The schematic procedures of the sampling are shown in Fig. 3(a). The cylindrical samples with a dimension of 30 cm in diameter and about 100 cm in height were retrieved vertically from the excavated base, as typically shown in Fig. 3(b). These samples were well-graded gravel with cobbles and boulders which were infilled with sandy and finer soils. By employing the above coring method, a smooth side surface of the samples could be achieved as typically shown in Fig. 3(c). Large-scale specimens with a dimension of 30 cm in diameter and 60 cm in height were trimmed from the cylindrical samples. For the trimming work, the polymer that has been used for the coring work was also employed in combination with a cutting machine with a large-diameter disk blade as shown in Fig. 3(d). A smooth end of the specimens could also be achieved as shown in Fig. 3(c).

Medium-scale specimens with a dimension of 10 cm in diameter and 20 cm in height were obtained from the trimmed rest parts of large-scale samples, as typically illustrated in Fig. 3(e), by using the same coring and trimming methods as mentioned above.

At MT, the average overburden depth ranges from 4 to 6 m and the shallowest part is less than 3 m. Due to the low overburden pressure, chemical injection for the ground improvement was carried out before excavation in order to reduce the deformation caused by the construction. Cylindrical samples with a dimension of 16.5 cm in diameter and about 50 cm in height were retrieved horizontally from the excavated section before and after chemical injections, as typically shown in Fig. 4, by pushing steel tube samplers with a hydraulic powered backhoe. These samples were well-graded gravel with cobbles which were infilled with sandy and finer soils. Medium-scale specimens with a dimension of 10 cm in diameter and 20 cm in height were trimmed from the

Table 1
List of the specimens tested in the present study and those referred to in this paper.

Material	Specimen code	Test condition		Drainage condition	ρ_d (g/cm^3)	d (mm)	D_{max} (mm)	D_{50} (mm)	U_c	FC (%)	$\sigma_3'=\sigma_h'$ (kPa)	Travel time	Remarks
First Uozu Tunnnel	FU-L-1	TC	S	D	[a]	300	140	31.09	170.6	2.6	400	Rise	Present study
First Uozu Tunnnel	FU-L-2	TC	S	D	1.92	300	160	41.53	156.0	1.9	400	Rise	Present study
First Uozu Tunnnel	FU-L-3	TC	S	D	2.11	300	130	48.19	148.8	1.9	400	Rise	Present study
First Uozu Tunnnel	FU-L-4	TC	S	D	2.04	300	130	37.94	124.4	2.1	400	Rise	Present study
First Uozu Tunnnel	B1	TC	US	D	2.07	300	[b]	[b]	[b]	[b]	80	Peak	Koseki et al. (2011)
First Uozu Tunnnel	B2	TC	US	D	2.10	300	[b]	[b]	[b]	[b]	200	Peak	Koseki et al. (2011)
First Uozu Tunnnel	B3	TC	US	D	2.11	300	182	27.1	132.4	3.5	400	Peak	Koseki et al. (2011)
Second Uozu Tunnnel	SU-L-1	TC	US	D	2.05	300	250	72.4	107.6	1.0	80	Rise	Present study
Second Uozu Tunnnel	SU-L-2	TC	S	D	2.05	300	220	42.35	125.0	1.6	200	Rise	Present study
Second Uozu Tunnnel	SU-L-3	TC	US	D	2.11	300	200	70.49	232.2	1.6	400	Rise	Present study
Second Uozu Tunnnel	SU-L-7	TC	S	D	2.06	300	260	49.13	119.2	1.3	400	Rise	Present study
Second Uozu Tunnnel	SU-L-8	TC	S	D	2.13	300	290	83.86	62.5	1.3	400	Rise	Present study
Second Uozu Tunnnel	SU-L-4	UC	US	D	[c]	300	290	87.56	212.6	1.6	0	Rise	Present study
Second Uozu Tunnnel	SU-L-5	UC	US	U	2.05	300	260	83.32	184.2	1.1	0	Rise	Present study
Second Uozu Tunnnel	SU-M-7	UC	S	U	2.16	100	[b]	[b]	[b]	[b]	0	Rise	Present study
Second Uozu Tunnnel	SU-M-8	UC	S	U	2.10	100	[b]	[b]	[b]	[b]	0	Rise	Present study
Makurano Tunnnel (Unimproved)	MK-B-1	TC	S	D	1.58	100	50.8	0.257	[d]	41.0	40	Peak	Present study
Makurano Tunnnel (Unimproved)	MK-B-2	TC	S	D	1.90	100	125	28.19	[d]	19.0	80	Peak	Present study
Makurano Tunnnel (Unimproved)	MK-B-3	TC	S	D	1.58	100	50.8	0.12	[d]	47.6	200	Peak	Present study
Makurano Tunnnel (Improved)	MK-A-1	TC	S	D	1.34	100	38.1	0.428	42.3	15.2	40	Peak	Present study
Makurano Tunnnel (Improved)	MK-A-2	TC	US	D	1.37	100	100	0.559	17.6	11.9	80	Peak	Present study
Makurano Tunnnel (Improved)	MK-A-3	TC	S	D	2.10	100	79.2	23.14	258.2	6.0	200	Peak	Present study
Shin-Oyashirazu Tunnnel	A1	TC	US	D	2.21	300	[b]	[b]	[b]	[b]	80	Peak	Koseki et al. (2011)
Shin-Oyashirazu Tunnnel	A2	TC	US	D	2.31	300	[b]	[b]	[b]	[b]	200	Peak	Koseki et al. (2011)
Shin-Oyashirazu Tunnnel	A3	TC	US	D	2.12	300	[b]	[b]	[b]	[b]	400	Peak	Koseki et al. (2011)
Shin-Oyashirazu Tunnnel	A4	TC	US	D	2.23	300	162	41.6	26.8	1.3	80	Peak	Koseki et al. (2011)
Toyoura sand	TY-L-1	TC	A	D	1.62	300	0.425	0.196	1.65	0	400	Rise	Present study
Toyoura sand	TY-L-2	TC	A	D	1.62	300	0.425	0.196	1.65	0	400	Rise	Present study
Toyoura sand	TY-L-3	TC	A	D	1.61	300	0.425	0.196	1.65	0	400	Rise	Present study
Toyoura sand	T1–T7	TC	S or A	D	1.46–1.60	50	0.425	0.196	1.65	0	400	Rise	Wicaksono (2007)
Toyoura sand	TC4–TC7	True TC	A	D	1.61–1.63	265[e]	0.35	0.21	1.7	0	100	Peak	Maqbool et al. (2011)
Chiba gravel	TC1–TC3 TC11–TC15	True TC	M	D	1.91–2.17	265[e]	38	11.0	30.0	0	100	Peak	Maqbool et al. (2011)
Hime gravel	H1–H10	TC	S or A	D	1.57–1.76	50	4.75	1.716	2.06	0	400	Rise	Wicaksono (2007)

TC: Triaxial compression, UC: Unconfined compression, S: Saturated, US: Unsaturated, A: Air-dried, M: Moist (w_{ini}=5.5%), D: Drained, U:Undrained.
[a]Missing.
[b]Sieve analyses were not conducted.
[c]Not obtained due to large boulders.
[d]The value of D_{10} was not obtained.
[e]Equivalent diameter evaluated by assuming that an equivalent cylindrical specimen has the same cross-sectional area as a prismatic one.

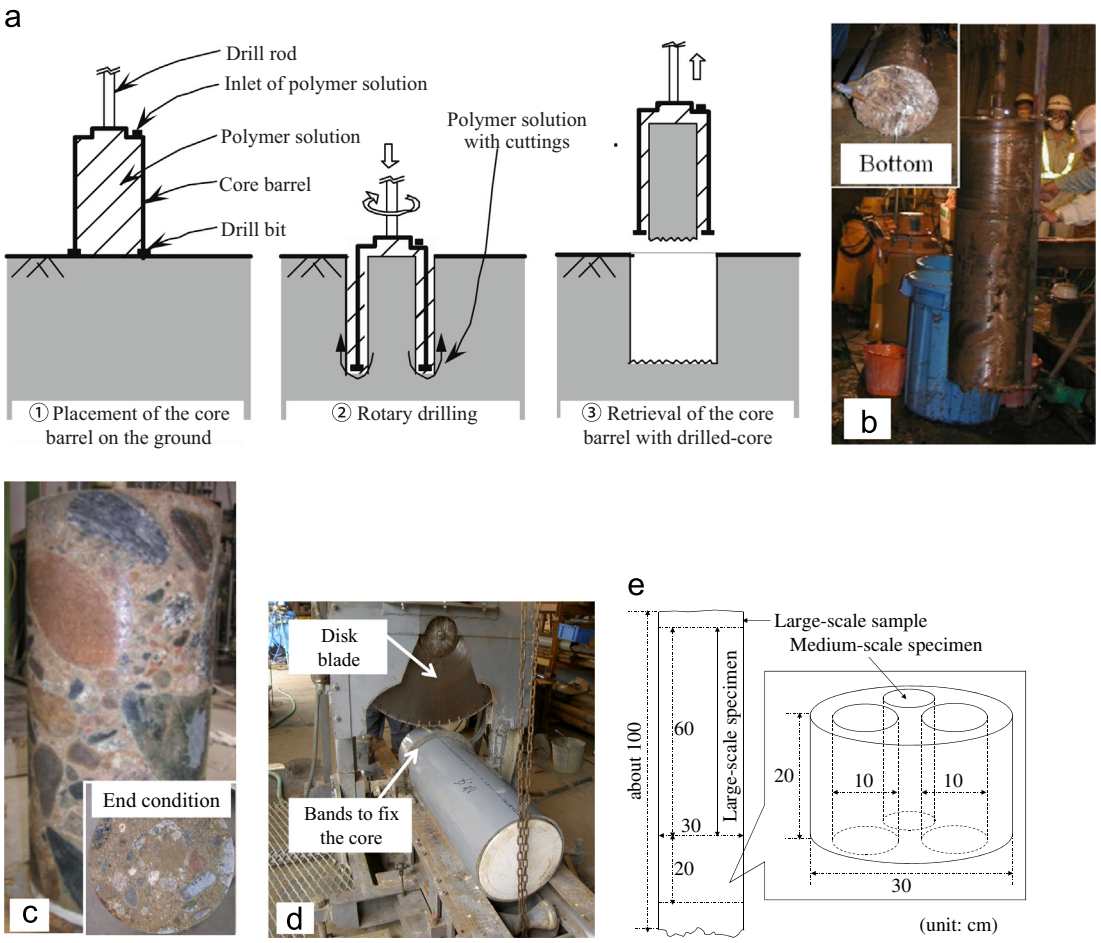

Fig. 3. Retrieval of UGS samples: (a) schematic procedures of sampling (Tani et al., 2007), (b) retrieval of core barrel, (c) typical side surface and end condition of large-scale specimen, (d) core cutter and (e) schematic diagram of retrieval of medium-scale specimens.

cylindrical samples by the same method as mentioned above. A comparison of the test results obtained from both unimproved (without/before chemical injection- virgin) and improved (after chemical injection) specimens is also included in this paper.

3. Test apparatus and procedure

An automated large-scale triaxial apparatus as illustrated in Fig. 5 was used. It was also used for medium-scale specimens. The axial loading device consists of a computer-controlled hydraulic actuator with a capacity of 490 kN and a computer-controlled high precision gear-type axial loading system. The axial load was measured with a load cell placed inside the triaxial cell to eliminate the effects of piston friction. The vertical deformation was measured with an external displacement transducer (EDT). The effective confining pressure was measured with a high-capacity differential pressure transducer (HCDPT).

3.1. Undisturbed gravelly soils

The top and bottom ends of specimens were not lubricated but in contact with the rigid faces of the top cap and pedestal made of duralumin via a sheet of filter paper. The vertical deformation was measured also locally with three pairs of local deformation transducers (LDTs, Goto et al., 1991) for large-scale specimens, and with a pair of LDTs for medium-scale ones. The horizontal deformation was measured locally with three clip gages (CGs) for large-scale specimens and with two CGs for medium-scale ones. The volume change of the specimen was obtained by measuring the water height in a burette connected to the specimen by using a low-capacity differential pressure transducer (LCDPT). The volumetric strain, ε_{vol}, of the specimen can also be obtained from Eq. (1) using the vertical and horizontal strains, ε_v and ε_h, measured with LDTs and CGs respectively by assuming the deformation of the specimen was uniform.

$$\varepsilon_{vol} = \varepsilon_v + 2\varepsilon_h \tag{1}$$

The specimen was set into the triaxial apparatus and was made saturated under an effective mean stress $p' = (\sigma'_v + 2\sigma'_h)/3 = 20$ kPa for medium-scale UC tests and 30 kPa for the other tests by employing a double vacuuming method (Ampadu and Tatsuoka, 1993), where σ'_v and σ'_h are the effective vertical and horizontal principal stresses. In some tests, the specimens could not be fully saturated due to their lower permeabilities (i.e., unsaturated). However, it was assumed that the effects of the saturation conditions on the

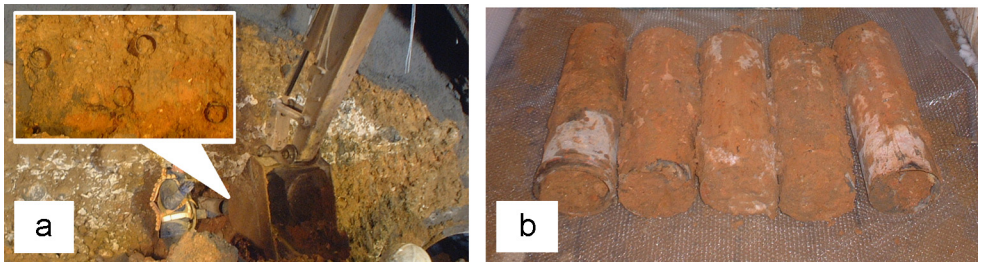

Fig. 4. Retrieval of UGS samples at MT: (a) core barrels pushed horizontally into excavated section and (b) retrieved samples with core barrels.

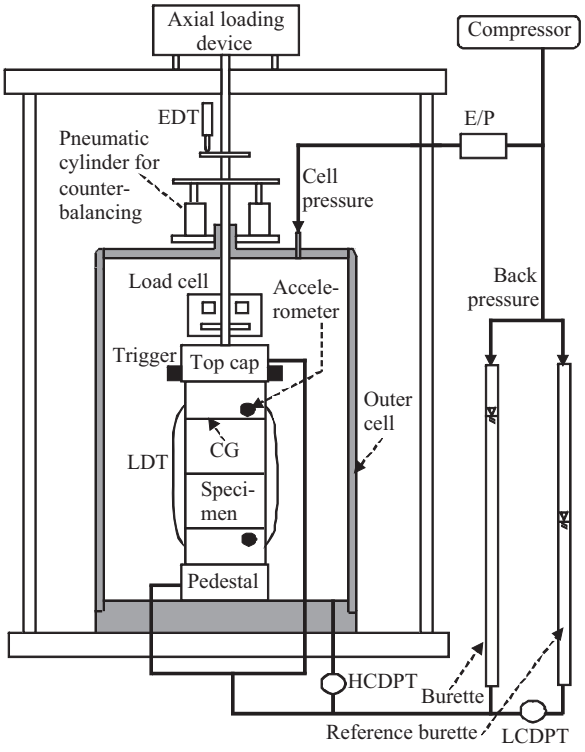

Fig. 5. Schematic diagram of testing apparatus.

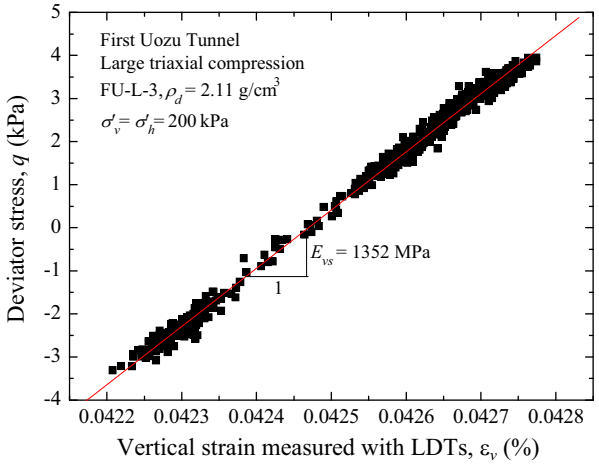

Fig. 6. Typical stress–strain relationship during vertical cyclic loading at small strain level.

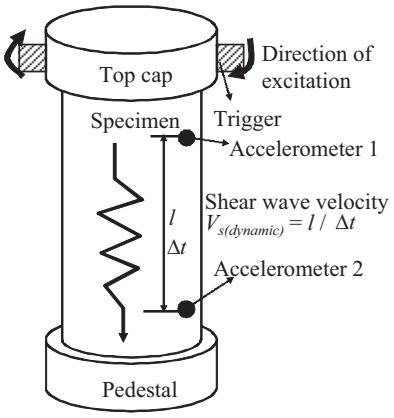

Fig. 7. Schematic diagram of testing equipment for dynamic measurement.

results obtained from drained tests were insignificant. In UC tests, drained or undrained strain-controlled shearing was conducted at the unconfined condition after unloading of the effective confining pressure. In TC tests, isotropic consolidation was employed for simplicity. The specimens were compressed to respective effective stress levels shown in Table 1 in an automated way using the axial loading device and an electro-pneumatic transducer for cell pressure. After isotropic consolidation, strain-controlled or stress-controlled drained TC tests were started. In some tests, large amplitude unloading and reloading cycles were applied during shearing in order to evaluate deformation characteristics during these cycles.

At several stress states in the course of isotropic consolidation and shearing, in order to determine quasi-elastic vertical Young's moduli, E_{vs}, by static measurement, eleven cycles with double amplitude axial strain of the order of 0.001% were applied after drained sustained loading as typically shown in Fig. 6. The values of E_{vs} were found to depend predominantly on the current values of σ'_v as shown in Eq. (2) proposed by Tatsuoka and Kohata (1995).

$$E_{vs} = \left(\frac{\partial \sigma'_v}{\partial \varepsilon_v}\right)_{d\sigma'_h = 0} = E_{v0}\left(\frac{\sigma'_v}{\sigma'_0}\right)^m \tag{2}$$

where E_{v0} is a reference vertical Young's modulus at a reference stress state of $\sigma'_v = \sigma'_0$; and m is the parameter presenting the stress-state dependency of Young's moduli.

As a dynamic method, as schematically shown in Fig. 7, measurements of shear wave velocities were conducted at the side surface of the specimen by using a pair of piezo-electric accelerometers at the same stress levels as the static

measurements in a single test. Shear waves were generated by exciting the top cap in the torsional direction with a pair of multi-layerd piezo-electric triggers attached to the top cap (AnhDan et al., 2002) by inputting a single sinusoidal wave at the predominant frequency ranging from about 0.5 to 4 kHz. Those frequencies for each dynamic measurement were calculated by applying Fast Fourier Transform for the first half cycle of the single pulse wave which was recorded by the upper accelerometer. In this method, the trigger and the receiver do not need to be inserted into the specimens unlike the bender element, which can eliminate the disturbance of specimens mentioned in the introduction as well as bedding error. In fact, Wicaksono et al. (2008) reported that the values of shear modulus of Toyoura sand obtained with this method were about 30% higher than those with the bender element.

In order to reduce the noise levels in the measured data, a stacking technique was introduced by employing a built-in function of the digital oscilloscope. As shown in Maqbool et al. (2011), the wave signal becomes significantly clear with increasing the number of stacked signals. Following the recommendation made by them, stacking of 256 data for each dynamic measurement was conducted. To evaluate the travel time of shear wave, two methods were employed as typically shown in Fig. 8 (see Table 1). According to Maqbool et al. (2011), the rise-to-rise travel time, Δt_{rise}, was in general by about 2–5% larger than the peak-to-peak travel time, Δt_{peak}, under the test condition employed in the study. However, in the present study, it is assumed that the difference of these two methods would not cause significant difference in calculating the wave velocities. Based on elastic continuum mechanics, the shear moduli measured dynamically, G_{vhd}, were determined by

$$G_{vhd} = \rho_t V_{s(dynamic)}^2 \tag{3}$$

where ρ_t is the wet density of the specimen; and $V_{s(dynamic)}$ is the shear wave velocity obtained from the dynamic measurement.

In addition, in order to compare the results from dynamic and static measurements, the values of E_{vs} obtained from static measurements are converted into those of shear moduli, G_{vhs}, by using Eq. (4) which was originally proposed by Tatsuoka et al. (1999).

$$G_{vhs} = \frac{E_{vs}}{2(1+\upsilon_0)} \frac{2(1-\upsilon_0)}{1+aR^m-2\sqrt{a}R^{m/2}\upsilon_0} \tag{4}$$

where υ_0 is the Poisson's ratio at isotropic stress states (set equal to 0.35 for all the specimens retrieved from MT as an average value of the test data, and 0.25 for those retrieved from FUT and SUT based on the assumption employed by Koseki et al., 2011); a is a parameter on inherent anisotropy (set equal to 1.0 in the present study, for simplicity, by neglecting the effects of inherent anisotropy); R is the effective principal stress ratio defined as σ'_v/σ'_h; and m is the parameter defined by Eq. (2).

3.2. Toyoura sand

Large-scale specimens with a dimension of 30 cm in diameter and 60 cm in height were produced by the air-pluviation method to reach high density (initial relative density

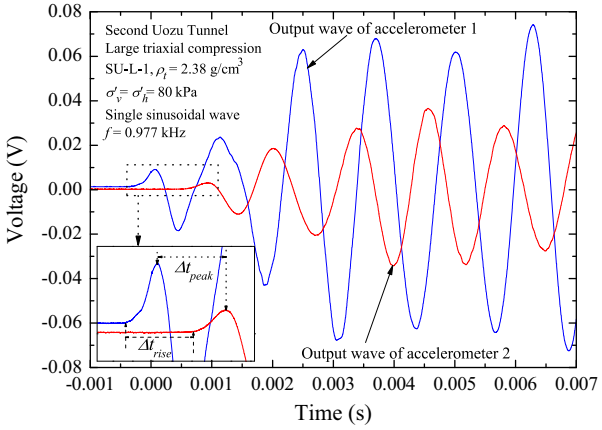

Fig. 8. Definition of wave travel time.

D_{r0} = about 95%). In order to investigate the effects of bedding error on the small strain properties by the static and dynamic measurements, two end conditions of the specimens were employed. In case of tests TY-L-1 and 2, the top and bottom ends of specimens were in contact with the rigid faces of the top cap and pedestal made of duralumin via a sheet of filter paper. On the other hand, with test TY-L-3, the top and bottom ends were well-lubricated by using a 0.8 mm-thick latex rubber smeared with a 0.05 mm-thick silicone grease layer (Tatsuoka et al., 1984). After isotropic compression was performed from p' = 50 kPa towards 400 kPa while keeping the specimen under air-dried condition, strain-controlled or stress-controlled drained TC tests were executed. The vertical and horizontal deformations were measured locally with three pairs of LDTs and three CGs respectively. At several stress states in the course of isotropic consolidation and shearing, static and dynamic measurements were conducted. In the dynamic measurement, a single sinusoidal wave at a frequency ranging from about 1 to 4 kHz was inputted. For calculating the values of ρ_t used in Eq. (3), the volume change of the specimen was evaluated based on measurements of vertical and horizontal deformations. In test TY-L-2 that was conducted to evaluate the peak strength, the volumetric strain during shearing was estimated by substituting measured R values and axial strain increments into the modified Rowe's stress-dilatancy relation (see Appendix B of Tatsuoka et al., 2008) calibrated by measurements based on LDTs and CGs in the same specimen, due to their limited capacities of measurements.

4. Test results and discussions

4.1. Strength and deformation characteristics

Fig. 9 shows the results obtained from three drained TC tests and a drained UC test at a constant vertical strain rate ($\dot{\varepsilon}_v$) of ± 0.08%/min with respect to UGSs retrieved from SUT. The deviator stress, $q = \sigma'_v - \sigma'_h$, at the relatively small strain level of test SU-L-1 was the largest of four tests as shown in Fig. 9(a), while the peak strength tended to become larger with increasing horizontal effective stress. In all TC tests, large amplitude unloading and reloading cycles were applied at

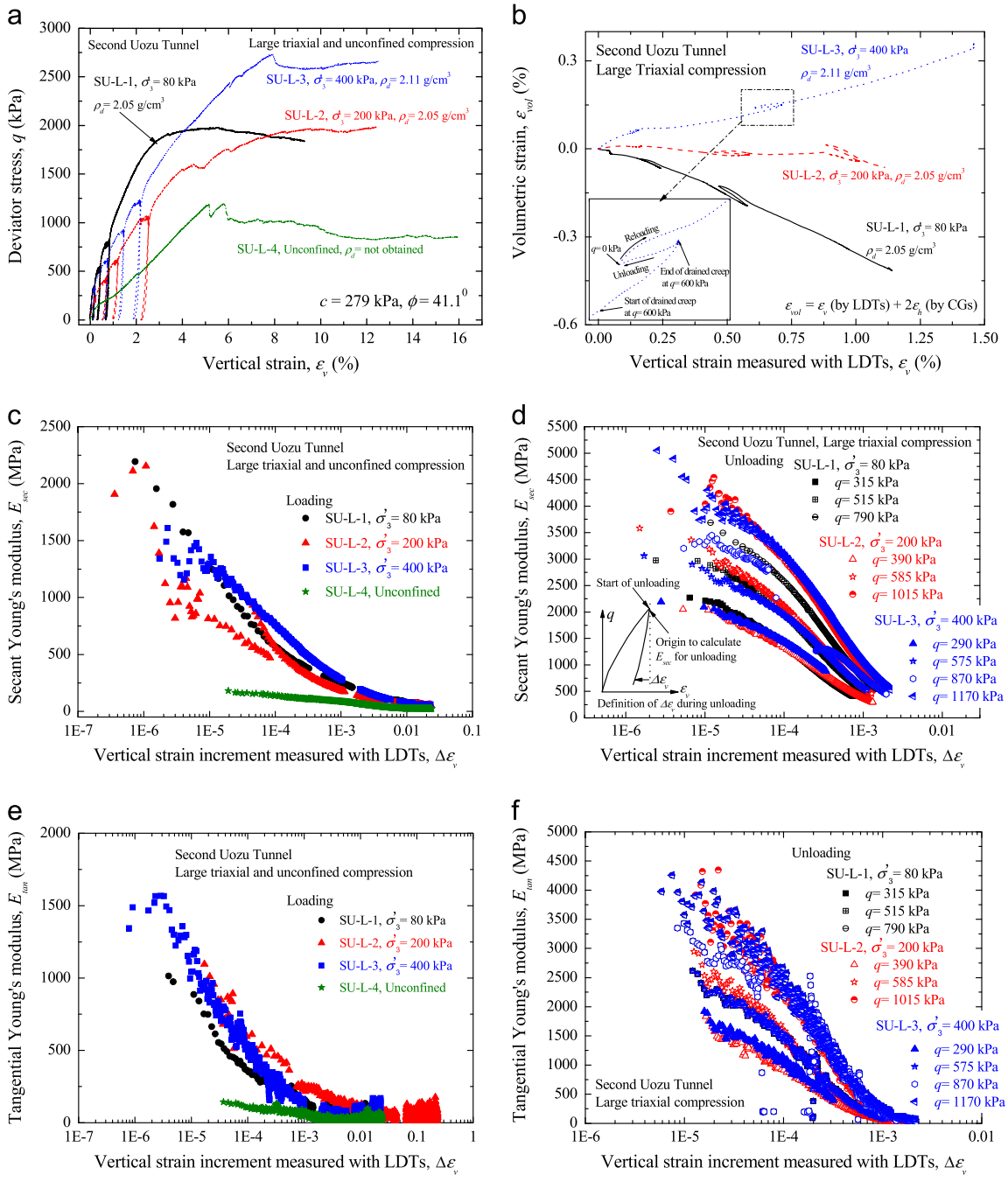

Fig. 9. Results obtained from drained TC and UC tests on UGSs retrieved from SUT: (a) whole strain range of $q-\varepsilon_v$ relation, (b) $\varepsilon_{vol}-\varepsilon_v$ relation based on measurements with LDTs and CGs, (c) and (d) strain dependency of secant Young's modulus, and (e) and (f) strain dependency of tangential Young's modulus.

different stress states during shearing. In case of test SU-L-3, the dilative behaviour was observed during the large amplitude unloading, while the contractive behaviour occurred when the reloading started (Fig. 9(b)). This behaviour trend was reversed for tests SU-L-1 and 2. Then, the $\varepsilon_{vol}-\varepsilon_v$ relation totally rejoined the original one during subsequent monotonic loading at a constant $\dot{\varepsilon}_v$. The strain dependency of secant and tangential Young's moduli based on measurements with LDTs are shown in Figs. 9(c) through (f), where the definition of vertical strain increment, $\Delta\varepsilon_v$, during unloading is schematically presented in Fig. 9(d). The non-linear behaviour of these two moduli was observed with increasing $\Delta\varepsilon_v$. The values of these two moduli during the large amplitude unloading were higher than those during loading respectively as compared at the same $\Delta\varepsilon_v$, which suggests that the higher elasticity was observed in unloading than loading. The values of secant Young's moduli were higher than those of tangential ones as compared at the same $\Delta\varepsilon_v$ excluding those at very small strain levels.

Fig. 10 shows the comparison of strength and deformation characteristics obtained from six drained TC tests at $\dot{\varepsilon}_v = \pm 0.08\%$/min with respect to UGSs retrieved from MT before and after chemical injections (unimproved and improved

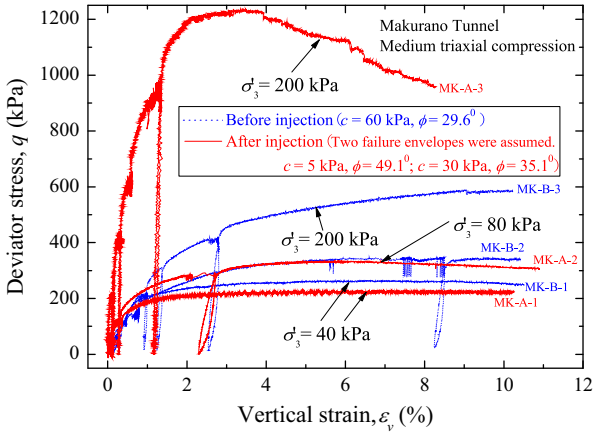

Fig. 10. Comparison of strength and deformation characteristics obtained from drained TC tests on UGSs retrieved from MT before and after chemical injections.

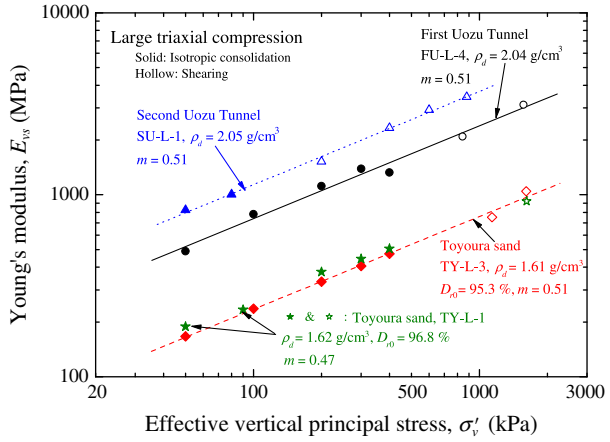

Fig. 11. Typical results showing stress-state dependency of E_{vs} of UGSs retrieved from FUT and SUT, and Toyoura sand.

specimens respectively). The peak strength of test MK-A-3 conducted under $\sigma'_h = 200$ kPa was extremely large, due possibly to large cobbles in the specimen and a high dry density shown in Table 1. Excluding this test result, the peak strength of improved specimens tended to be slightly lower than that of unimproved specimens. The possible factors which can explain this test result may be; (a) lower dry densities of improved specimens; (b) the distribution of larger particles within the specimens; and (c) the disturbance of the in-situ ground caused by having conducted the chemical injection. The strength properties of granular materials can be largely affected by the above factors (a) and (b) even if the specimens have similar grading curves. These inevitable scatters among different undisturbed specimens affected the test results obtained from the present study.

Holtz and Gibbs (1956) reported that the strength tended to increase with increasing maximum diameter D_{max} in drained TC tests on GSs. As pointed out by Imai et al. (1991), the peak internal friction angle tends to be overestimated for $D_{max}/d > 0.2$ in drained TC tests. Since this is the case for the investigated soils (see Table 1), the peak friction angle may have been overestimated.

4.2. Comparison between static and dynamic measurements

The typical results obtained from static measurements of UGSs retrieved from FUT and SUT and Toyoura sand are shown in Fig. 11, where E_{vs} is plotted versus σ'_v on a full logarithmic scale. The m values defined by Eq. (2) are indicated in Fig. 11. Since the difference between the results from tests TY-L-1 and 3 which employed the different end conditions was small, it can be seen that the effects of bedding error on the small strain properties by the static measurements were insignificant. All m values of the tested materials are plotted versus D_{50} in Fig. 12. Excluding some exceptional data, m seemed to be essentially constant on uncemented sands and gravels as summarized by Kohata et al. (1997) and Hoque and Tatsuoka (1998).

The typical results obtained from dynamic measurements of UGSs retrieved from FUT and SUT and Toyoura sand are shown in Fig. 13, where the values of G_{vhs} calculated back

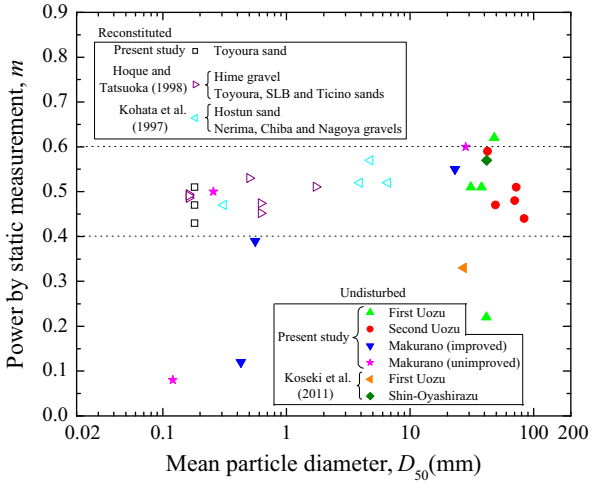

Fig. 12. Relationship between m and D_{50} of geomaterials including UGSs.

from E_{vs} shown in Fig. 11 by using Eq. (4) and G_{vhd} are plotted versus an effective stress parameter, $(\sigma'_v\sigma'_h)^{0.5}$, on a full logarithmic scale. As a result, since those moduli increased with increasing $(\sigma'_v\sigma'_h)^{0.5}$, Eq. (5) is employed.

$$G_{vh} = G_{vh0}\left(\frac{(\sigma'_v\sigma'_h)^{0.5}}{\sigma'_0}\right)^{m'} \quad (5)$$

where G_{vh0} is a reference shear modulus at a reference stress state of $(\sigma'_v\sigma'_h)^{0.5} = \sigma'_0$; and m' presents stress-state dependency of shear moduli. The m' values based on static and dynamic measurements, denoted as m_s' and m_d' respectively, are indicated in Fig. 13. Since the difference between the results from tests TY-L-2 and 3 which employed the different end conditions was small, it can be seen that the effects of bedding error on the small strain properties by the dynamic measurements were insignificant. It can be seen that the values of G_{vhd} were larger than those of G_{vhs} for all stress states and all geomaterials. It should also be noted that the difference between these two moduli of UGSs was larger than that of Toyoura sand.

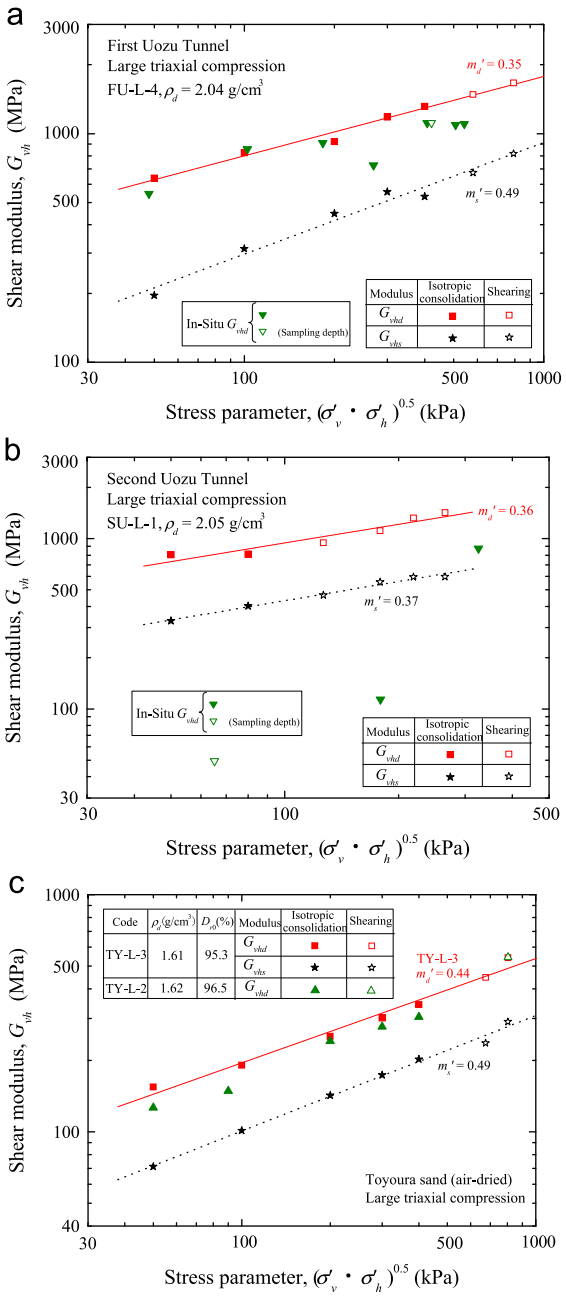

Fig. 13. Typical results showing stress-state dependency of G_{vhs} converted from E_{vs} and G_{vhd}: (a) and (b) UGSs retrieved from FUT and SUT, respectively, and (c) Toyoura sand.

This difference may have been caused by the effects of heterogeneity of the specimen on the dynamic measurement results as pointed out by Tatsuoka and Shibuya (1992) and confirmed by Tanaka et al. (2000), among others. In the dynamic measurement, since the wave travels through the shortest travel time path made by interlocking of larger particles, the shear modulus, which reflects the stiffest soil structure of the specimen, is obtained. It should be noted that the shear modulus based on static measurements reflects the average property of the overall specimen. Therefore, the former shear modulus tends to be larger than the latter one with heterogeneous materials. The difference between these two moduli tends to decrease with decreasing degree of heterogeneity of the specimen (Tanaka et al., 2000; AnhDan et al., 2002).

As another dynamic measurement, the results from the in-situ velocity logging tests for the primary and secondary waves (in-situ PS logging tests) that were conducted before the excavations at FUT and SUT are also plotted in Fig. 13, where the in-situ horizontal stress was evaluated, due to a lack of reliable data, by tentatively assuming that the coefficient of earth pressure at rest was 0.5. G_{vhd} based on the in-situ PS logging test result that corresponds to the sampling depth at FUT was rather consistent with that based on the dynamic measurement in the laboratory. On the other hand, when the data with respect to SUT are compared to the stress state that corresponds to the sampling depth, in-situ G_{vhd} was significantly lower than the values of shear moduli obtained from the static and dynamic measurements in the laboratory.

The above behaviour with respect to SUT may be explained by any of the following; (a) the effect of the heterogeneity of the in-situ ground; (b) the error in determining of the travel length in the in-situ PS logging tests; (c) the difference between the wave lengths employed in the in-situ and laboratory dynamic measurements; and (d) the densification of the samples caused during the coring process. The distance, L, between the sampling location and the borehole where the in-situ PS logging tests were conducted was about 200 m for SUT, while about 5 m for FUT. That is, at SUT, the soil properties of the specimens would be different from those of the in-situ ground where the PS logging tests were conducted, due to the above factor (a). The discussion on the above factor (c) will be made in the next section.

Fig. 14 shows the comparison of small strain properties obtained from six drained TC tests on UGSs retrieved from MT before and after chemical injections (unimproved and improved specimens respectively). In the static measurements, as shown in Fig. 14(a), similar lower limits of G_{vhs} were observed with and without chemical injections. The G_{vhs} values of test MK-A-3 were extremely large, possibly because of the same reason as discussed previously on the test results shown in Fig. 10. In the dynamic measurements, as shown in Fig. 14(b), similar lower limits of G_{vhd} were also observed with and without chemical injections. The m_d' values of unimproved specimens were larger than those of improved ones. Unlike the trend obtained from the static measurements, the G_{vhd} values of test MK-B-2 were extremely large owing possibly to a large cobble in the specimen shown in Fig. 14(a). This result suggests that an extremely large particle in the specimen affects the results from dynamic measurements more than the static ones. It should also be noted that G_{vhd} was greater than G_{vhs} for all stress states.

By assuming that the coefficient of earth pressure at rest was 0.5, the results from the in-situ PS logging tests that were conducted at one borehole close to the sampling location (L=about 5 m) before and after chemical injections are also plotted in Fig. 14(b). It can be seen that G_{vhd} at the sampling depth before chemical injection was higher than after chemical injection. This result suggests that the in-situ ground may have been disturbed by the chemical injection.

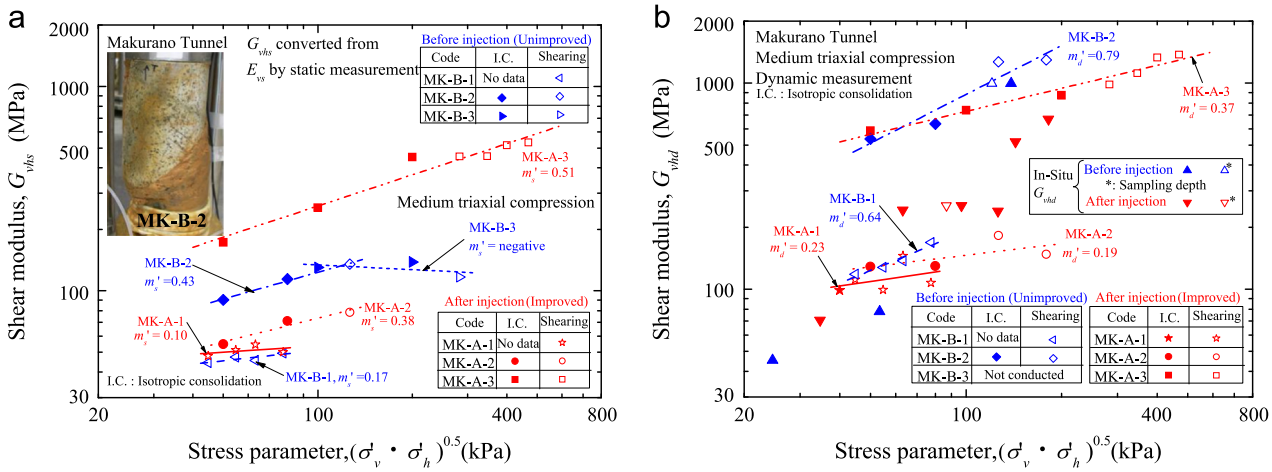

Fig. 14. Comparison of small strain properties in drained TC tests on UGSs retrieved from MT before and after chemical injections: (a) G_{vhs} converted from E_{vs} and (b) G_{vhd} from in-situ and laboratory dynamic measurements.

The G_{vhd} value based on the in-situ PS logging test that had been conducted at the sampling depth before chemical injection was rather consistent with that obtained from the laboratory dynamic measurement in test MK-B-2. On the other hand, the former value after chemical injection was between the lowest and highest values obtained from dynamic measurements in the laboratory.

4.3. Factors affecting difference between small strain properties based on static and dynamic measurements

In this section, several factors affecting the difference between the small strain properties based on the static and dynamic measurements are discussed. The results obtained from the present study and some previous studies shown in Table 1 are used for the following discussions.

The first factor is the stress level. Figs. 15(a) and (b) show the relationships between the ratios G_{vhd}/G_{vhs} obtained from drained TC tests and the stress parameters $(\sigma'_v\sigma'_h)^{0.5}$ at which those moduli were determined. In isotropic consolidation, the ratios G_{vhd}/G_{vhs} of Toyoura sand hardly varied while those of well-graded UGSs tended to decrease with increasing stress level. This behaviour trend was more clearly seen in Fig. 15(c), where the results from UC and TC tests are plotted versus $(\sigma'_v\sigma'_h)^{0.5}$ on a full arithmetic scale. On the other hand, the ratios G_{vhd}/G_{vhs} of some UGSs during shearing tended to increase due possibly to the newly developed interlocking of large particles. The reasons for such behaviour during isotropic consolidation can be explained as follows.

Fig. 16 shows the comparison between the values of m_s' and m_d'during isotropic consolidation. It can be seen that m_s' was greater than m_d' for most of the tests on UGSs while the former value was approximately equal to the latter one with Toyoura sand. That is, with UGSs, G_{vhs} increased significantly stronger than G_{vhd} during isotropic consolidation since the portion consisting of sandy and finer soils may have become stiffer with increasing effective confining pressure as illustrated in Fig. 17(a). Consequently, the ratios G_{vhd}/G_{vhs} decreased with increasing stress level. Since the soil structure of Toyoura sand may have not changed largely during isotropic consolidation due to its higher uniformity as illustrated in Fig. 17(b), G_{vhd} and G_{vhs} increased in a similar manner with increasing effective confining pressure.

That is, the data shown in Fig. 15 suggest that heterogeneity of UGSs may have disappeared gradually and small strain stiffness of the overall UGS specimen tended to be uniformized during isotropic consolidation. The higher sensitivity of the static measurements than the dynamic measurements reflects that the small strain stiffness of well-graded granular materials is uniformized with an increase in the pressure level.

The second factor is the dry density. Fig. 18 shows the relationship between the ratios G_{vhd}/G_{vhs} measured at the isotropic stress state, $\sigma'_v=\sigma'_h=50$ kPa, in drained TC tests, $(G_{vhd}/G_{vhs})_{50}$, and the values of ρ_d. With the test cases that the ratio $(G_{vhd}/G_{vhs})_{50}$ was not evaluated experimentally, the interpolated or extrapolated ratios are plotted in Fig. 18. When the values of ρ_d and U_c exceeded at least approximately 1.9 g/cm^3 and 30, respectively, the ratios $(G_{vhd}/G_{vhs})_{50}$ tended to decrease with increasing ρ_d. The reason for this behaviour might be that G_{vhs} of well-graded GSs increases more remarkably with the densification than G_{vhd} as compared with poorly graded sands, due to larger uniformity coefficients. Maqbool et al. (2011) reported that the difference between Young's moduli of well-graded reconstituted GS measured statically and dynamically was also reduced by increasing dry density of the specimen in drained TC tests.

The third factor is the grading property. Fig. 19 shows the ratios $(G_{vhd}/G_{vhs})_{50}$ plotted versus; (a) D_{max}/d; (b) D_{50}/d; and (c) U_c. With the test cases that the ratio $(G_{vhd}/G_{vhs})_{50}$ was not evaluated experimentally, the interpolated or extrapolated values are plotted in Fig. 19. The dashed lines show the data range of geomaterials with relatively high densities ($\rho_d \geq 2.0$ g/cm^3). Due to the scatter of test data, possibly caused by the effect of the initial dry density mentioned above, and/or the heterogeneity of UGSs, no clear tendency could be observed. However, in general, the values of $(G_{vhd}/G_{vhs})_{50}$ tended to increase with increasing D_{max}/d, D_{50}/d and U_c. That is, the larger grain size and larger uniformity coefficient of soil

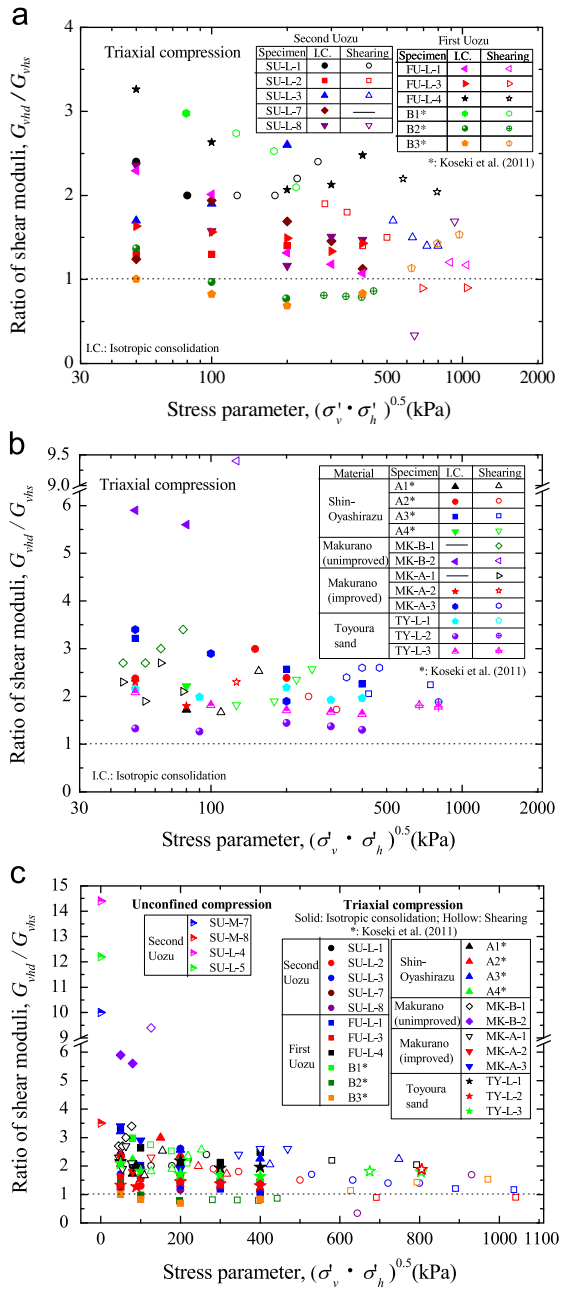

Fig. 15. Effects of stress level on G_{vhd}/G_{vhs}: (a) and (b) results from TC tests and (c) results from UC and TC tests.

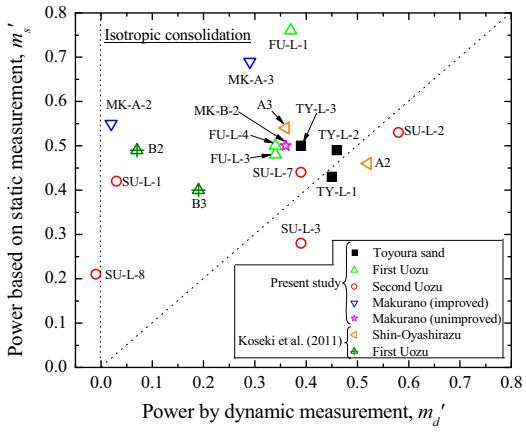

Fig. 16. Comparison between m' based on static and dynamic measurements.

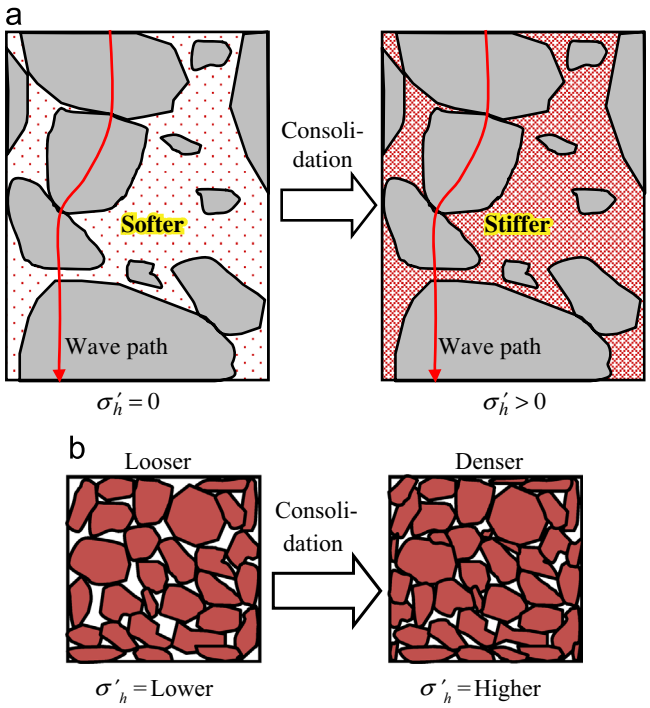

Fig. 17. Changes in the soil structures with an increase in the pressure level during isotropic consolidation in case of: (a) well-graded UGS and (b) Toyoura sand.

seem to lead to a larger modulus when measured dynamically rather than statically. The effects of the grading characteristics on the small strain properties of geomaterials have not been systematically studied and are not well understood, so further studies on this issue should be carried out.

The last factors are the wave length and particle size. Tanaka et al. (2000) and AnhDan et al. (2002) reported that the difference between static and dynamic measurements in terms of wave velocities was affected by the ratios $D_{50}/(\lambda/2)$, where λ is the wave length in the dynamic measurement. Fig. 20 shows the relationship between the ratios $V_{s(static)}/V_{s(dynamic)}$ and $D_{50}/(\lambda/2)$, where $V_{s(static)}$ is the equivalent shear wave velocity that is determined from G_{vhs} by replacing G_{vhd} and $V_{s(dynamic)}$ with G_{vhs} and $V_{s(static)}$ respectively in Eq. (3). The values of λ were computed based on the measured wave form, using the same definition as used by Tanaka et al. (2000).

In Fig. 20(a), the data from the laboratory tests are scattered largely even after taking the above-mentioned effects of the dry density into account. However, the trends of UGSs in the present study were similar to those of UGSs retrieved by the in-situ freezing method by Tanaka et al. (2000) and reconstituted GSs by AnhDan et al. (2002) and Maqbool et al. (2011).

The results from evaluation using the values of $V_{s(dynamic)}$ and λ obtained from the in-situ PS logging test results corresponding to the respective sampling depths are also plotted in Fig. 20(a), where the values of $V_{s(static)}$ corresponding to the respective sampling

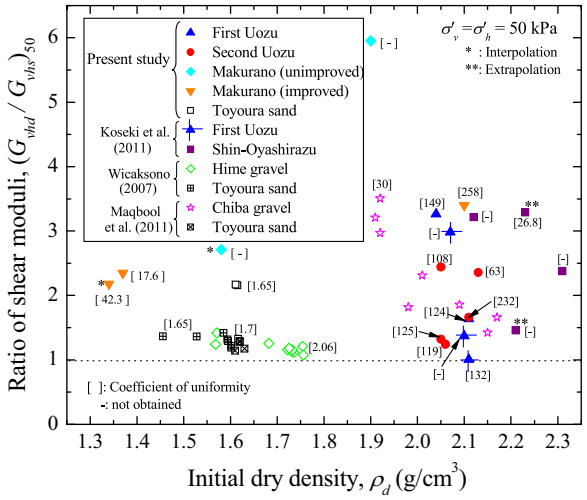

Fig. 18. Effects of dry density on G_{vhd}/G_{vhs} at $\sigma'_v=\sigma'_h=50$ kPa.

depths were interpolated or extrapolated from the respective $G_{vhs}-(\sigma'_v\sigma'_h)^{0.5}$ relations. The possible factors causing the scatter of these data may be attributed to any of the following; (a) inevitable scatters among different undisturbed specimens; and (b) the larger heterogeneity causing the difference between soil properties of specimens and those of the in-situ ground.

However, when the in-situ and laboratory data of tests FU-L-1, 3 and 4, MK-A-3, and A4 are compared respectively, it can be observed that the ratios $V_{s(static)}/V_{s(dynamic)}$ decreased with increasing $D_{50}/(\lambda/2)$. This result suggests that shear moduli measured dynamically tend to approach those measured statically when λ is significantly larger than D_{50}.

As discussed in Fig. 15 and shown in Fig. 20(b), the ratio $D_{50}/(\lambda/2)$ was not the only parameter that affects the ratio $V_{s(static)}/V_{s(dynamic)}$, the pressure level was also important factor. The ratios $V_{s(static)}/V_{s(dynamic)}$ of well-graded GSs tend to increase with increasing pressure level.

For accurately predicting the deformation behaviour of the ground in both the static and dynamic problems, small strain properties as well as strength and deformation characteristics should be evaluated properly. The analyses shown in this section suggest that, since small strain properties of in-situ shallow and loose gravelly layers evaluated by the dynamic measurements using shorter wave lengths may be significantly overestimated, due attention should be paid. On the other hand, if those properties of dense GSs are evaluated under higher stress levels by using longer wave lengths, the difference between shear moduli measured statically and dynamically may be negligible, which suggests that those properties based on the static methods can be employed in the dynamic analysis. Further studies will be necessary for a rational determination of the small strain properties which should be used in the deformation analysis.

4.4. Relationships between small strain and strength properties

According to Kim et al. (1991) who compiled the data obtained by many researchers, a good correlation between the maximum secant Young's modulus E_{max}, defined at very small

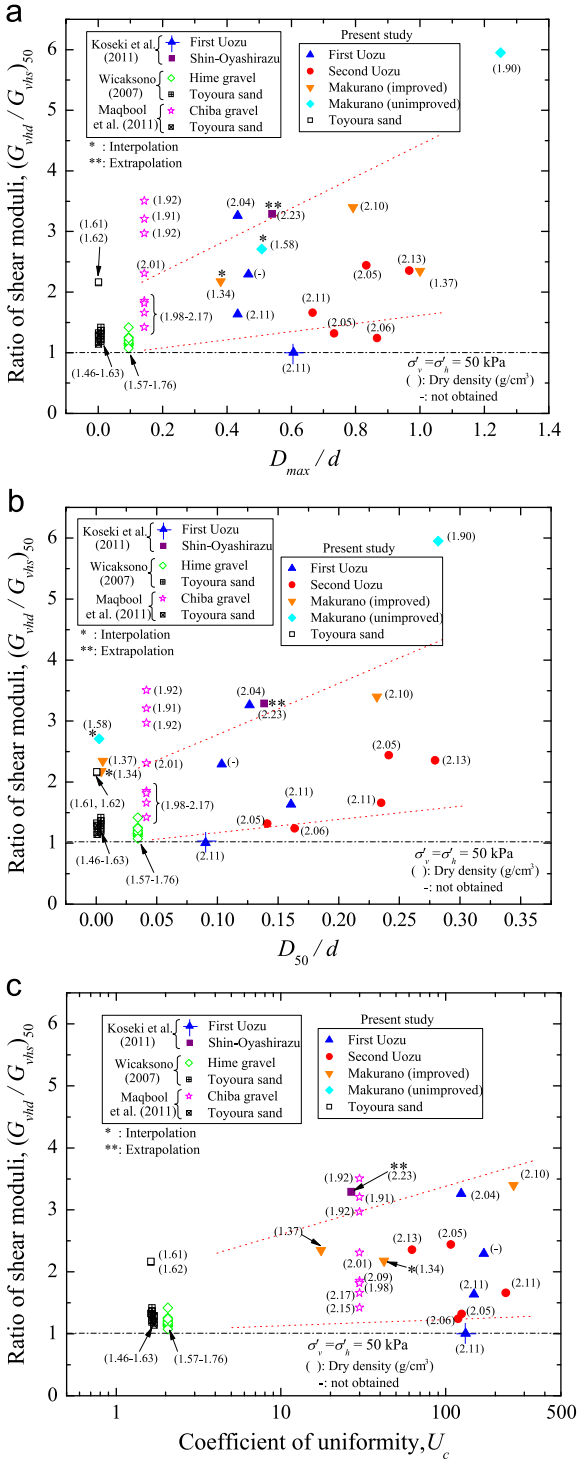

Fig. 19. G_{vhd}/G_{vhs} at $\sigma'_v=\sigma'_h=50$ kPa plotted versus: (a) D_{max}/d, (b) D_{50}/d and (c) U_c.

strains (about 10^{-5} or less), and the maximum deviator stress q_{max} can be seen for natural geomaterials (soft and stiff clays, sands, gravels and sedimentary soft and hard rocks) in laboratory stress–strain tests. The ratios E_{max}/q_{max} were approximately 1000 for uncemented soils and approximately 500 for soft and hard rocks.

Fig. 21 shows the relationship between E_{max} based on the static measurement with LDTs and q_{max} obtained from TC and

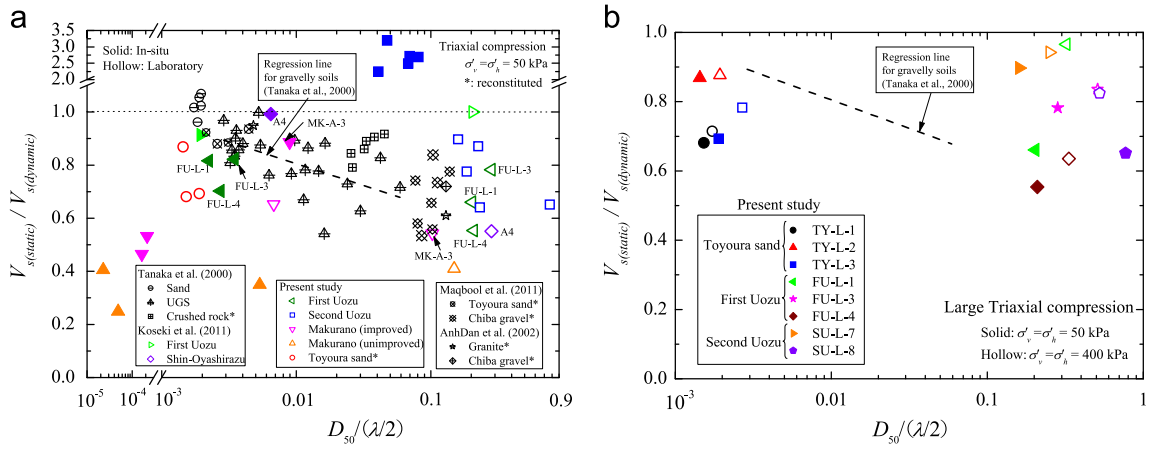

Fig. 20. Effects of particle size and wave length on $V_{s(static)}/V_{s(dynamic)}$ (modified from Tanaka et al., 2000; AnhDan et al., 2002; Maqbool et al., 2011): (a) comparison between laboratory and in-situ test results and (b) comparison between laboratory test results at two different stress states.

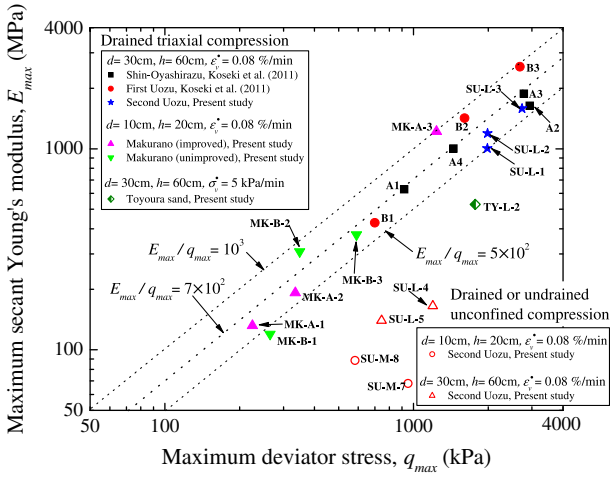

Fig. 21. Relationship between E_{max} and q_{max} of UGSs and Toyoura sand.

UC tests on UGSs and a TC test on Toyoura sand. The scatter of the data of UC tests were possibly caused by the larger heterogeneity of UGSs and the difference in the drainage conditions during shearing (see Table 1). It was shown that the ratios E_{max}/q_{max} of UGSs obtained from drained TC tests were between 500 (*behaviour of soft and hard rocks*) and 1000 (*behaviour of uncemented soils*), averagely 700. Since the difference between the static strength properties of the undisturbed and reconstituted gravelly specimens can be assumed to be insignificant as confirmed by Goto et al. (1992), the small strain properties of in-situ gravelly layers can be estimated roughly from q_{max} of the reconstituted ones by using the relationship shown in Fig. 21.

Since saturated cohesionless GSs should theoretically exhibit no unconfined strength, the data from the UC tests suggest that the cementation was developed among the soil particles of UGSs. These natural aging effects (i.e., cementation) on the small strain properties of GSs have been confirmed by Nishio and Tamaoki (1988) and Goto et al. (1992), who reported that the shear moduli of the reconstituted specimens were about 20–50% smaller than those of the undisturbed ones. For the accurate evaluation of the deformation behaviour of the ground, the effects of sample disturbance on the laboratory test results should be taken into account.

5. Conclusions

The following conclusions can be derived from the test results and analyses shown in this paper:

1. The values of shear moduli converted from vertical Young's moduli measured with static method (G_{vhs}) were smaller than those measured with dynamic method (G_{vhd}). The difference between the values of G_{vhd} and G_{vhs} of undisturbed gravelly soils (UGSs) tended to be larger than Toyoura sand, due to larger heterogeneity of UGSs. During isotropic consolidation, the ratios G_{vhd}/G_{vhs} of Toyoura sand hardly varied while those of UGSs tended to decrease with increasing stress level. This observation suggests that the shear moduli may be significantly overestimated when small strain properties of in-situ shallow gravelly layers are determined by the laboratory dynamic measurements.
2. When dry density and uniformity coefficient exceeded at least approximately 1.9 g/cm^3 and 30, respectively, the ratios G_{vhd}/G_{vhs} of well-graded undisturbed and reconstituted gravelly soils tended to decrease with increasing dry densities.
3. Increasing grain size and uniformity coefficient seemed to influence G_{vhd} more than G_{vhs}.
4. Some in-situ and laboratory data of UGSs suggested that, when the wave lengths were significantly larger than mean diameter, shear moduli measured dynamically tended to approach the ones measured statically.

Acknowledgements

The authors express their sincere thanks to Japan Railway Construction, Transport and Technology Agency for providing the undisturbed samples with relevant information, including the PS logging data. Kind assistance of Messrs. Yukawa, H.

and Kaneko, S. at Kiso-Jiban Consultants, Co. Ltd. in trimming the specimens is deeply appreciated.

References

Ampadu, S.K., Tatsuoka, F., 1993. Effects of setting method on the behavior of clays in triaxial compression from saturation on undrained shear. Soils Found. 33 (2), 14–34.

AnhDan, L., Koseki, J., Sato, T., 2002. Comparison of young's moduli of dense sand and gravel measured by dynamic and static methods. Geotech. Test. J. 25 (4), 349–368.

Brignoli, E.G.M., Gotti, M., Stokoe II, K.H., 1996. Measurement of shear waves in laboratory specimens by means of piezoelectric transducers. Geotech. Test. J. 19, 384–397.

Fioravante, V., 2000. Anisotropy of small strain stiffness of Ticino and Kenya sands from seismic wave propagation measured in triaxial testing. Soils Found. 40 (4), 129–142.

Goto, S., Tatsuoka, F., Shibuya, S., Kim, Y.-S., Sato, T., 1991. A simple gauge for local small strain measurements in the laboratory. Soils Found. 31 (1), 169–180.

Goto, S, Suzuki, Y., Nishio, S., Oh-oka, H., 1992. Mechanical properties of undisturbed Tone-river gravel obtained by in-situ freezing. Soils Found. 32 (3), 15–25.

Holtz, W.G., Gibbs, H.J., 1956. Triaxial shear tests on previous gravelly soils. J. Soil Mech. Found. Div. Proc. ASCE 82 (SM1), 1–22.

Hoque, E., Tatsuoka, F., 1998. Anisotropy in the elastic deformation of materials. Soils Found. 38 (1), 163–179.

Imai, G., Pradhan, T.B.S., Kamata, K, 1991. Scale effects on shear characteristics of granular materials. In: Proceedings of the 46th Japanese National Conference on Civil Engineering, pp. 444–445 (in Japanese).

Jardine, R.J., Potts, D.M., 1988. Hutton tension leg platform foundations: an approach to the prediction of pile behaviour. Geotechnique 38 (2), 223–228.

Jiang, G.L., Tatsuoka, F., Flora, A., Koseki, J., 1997. Inherent and stress-state-induced anisotropy in very small strain stiffness of a sandy gravel. Geotechnique 47 (3), 509–521.

Kim, Y-S., Shibuya, S., Ochi, K., Shi, D.-M., Tatsuoka, F., 1991. Deformation modulus and strength of artificial and natural soft rocks at low strain levels. In: Proceedings of the Symposium on Triaxial Testing Methods, JSSMFE, Tokyo, pp. 265–272 (in Japanese).

Kohata, Y., Tatsuoka, F., Wang, L., Jiang, G.J., Hoque, E., Kodaka, T., 1997. Modelling the non-linear deformation properties of stiff geomaterials. Geotechnique 47 (3), 563–580.

Koseki, J., Qureshi, O., Maqbool, S., Sato, T., Miyashita, Y.,Kuwano, R.,2011. Small strain properties of undisturbed gravelly soils retrieved from tunnel excavation sites in Japan. In: Proceedings of the International Symposium on Deformation Characteristics of Geomaterials, Seoul, Korea, pp. 266–271.

Leong, E.C., Yeo, S.H., Rahardio, H., 2005. Measuring shear wave velocity using bender elements. Geotech. Test. J. 28 (5), 488–498.

Maqbool, S., Kuwano, R., Koseki, J., 2011. Improvement and application of a P-wave measurement system for laboratory specimens of sand and gravel. Soils Found. 51 (1), 41–52.

Nishio, S., Tamaoki, K., 1988. Measurement of shear wave velocities in diluvial gravel samples under triaxial conditions. Soils Found. 28 (3), 35–48.

Okuyama, Y., Yoshida, T., Tatsuoka, F., Koseki, J., Uchimura, T., Sato, N., Oie, M., 2003. Shear banding characteristics of granular materials and particle size effects on the seismic stability of earth structures. In: Di Benedetto, H., Doanh, T., Geoffroy, H. Sauzeat, C. (Eds.), Deformation Characteristics of Geomaterials, vol. 1, pp. 607–616.

Tanaka, Y., Kudo, K., Nishi, K., Okamoto, T., Kataoka, T., Ueshima, T., 2000. Small strain characteristics of soils in Hualien, Taiwan. Soils Found. 40 (3), 111–125.

Tani, K., Kaneko, S., Sakai, K., 2007. Undisturbed sampling method using thick water-soluble polymer solution. In: Proceedings of the 13th Asian Regional Conf. on Geotechnical Engineering and Soil Mechanics, Kolkata, vol. 1, pp. 93–96.

Tatsuoka, F., Molenkamp, F., Torii, T., Hino, T., 1984. Behavior of lubrication layers of platens in element tests. Soils Found. 24 (1), 113–128.

Tatsuoka, F., Shibuya, S., 1992. Deformation characteristics of soils and rocks from field and laboratory tests, Keynote Lecture for Session No. 1. In: Proceedings of the 9th Asian Regional Conference on SMFE, Bangkok, vol. II, pp. 101–170.

Tatsuoka, F., Kohata, Y., 1995. Stiffness of hard soils and soft rocks in engineering applications. In: Pre-failure Deformation of Geomaterials, Sapporo, Japan, Balkema, vol. 2, pp. 947–1043.

Tatsuoka, F., Ishihara, M., Uchimura, T., Gomes Correia, A., 1999. Non-linear resilient behaviour of unbound granular materials predicted by the cross-anisotropic hypo-quasi-elasticity model. In: Correia (Eds.), Proceedings of the Workshop on Modelling and Advanced testing for Unbound Granular Materials, Lisboa, Balkema, pp. 197–204.

Tatsuoka, F., Di Benedetto, H., Enomoto, T., Kawabe, S., Kongkitkul, W., 2008. Various viscosity types of geomaterials in shear and their mathematical expression. Soils Found. 48 (1), 41–60.

Yasuda, N., Nakamura, A., Ohta, N., 1994. Deformation characteristics of undisturbed riverbed gravel by in situ freezing sampling method. In: Shibuya, S., Mitachi, T, Miura, S (Eds.), Pre-Failure Deformation of Geomaterials, Sapporo, Japan, vol. 1. Balkema, pp. 41–46.

Wicaksono, R.I., 2007. Small Strain Stiffness of Sand and Gravel Based on Dynamic and Static Measurements (Master thesis), University of Tokyo.

Wicaksono, R.I., De Silva, L.I.N., Mulmi, S., Enomoto, T., Kiyota, T., Tsutsumi, Y., Kuwano, R., Koseki, J., 2008. Small strain stiffness of Toyoura sand obtained from various techniques in IIS. Seisan Kenkyu 60 (6), 561–564.